Laminar mixing in a SMX static mixer evaluated by positron emission particle tracking (PEPT) and magnetic resonance imaging (MRI)

Mihailova, Olga; Lim, Victor; Mccarthy, Michael J.; Mccarthy, Kathryn L.; Bakalis, Serafim

DOI:
10.1016/j.ces.2015.07.015

Document Version
Publisher's PDF, also known as Version of record

Citation for published version (Harvard):
Mihailova, O, Lim, V, Mccarthy, MJ, Mccarthy, KL & Bakalis, S 2015, 'Laminar mixing in a SMX static mixer evaluated by positron emission particle tracking (PEPT) and magnetic resonance imaging (MRI)', Chemical Engineering Science, vol. 137, pp. 1014-1023. https://doi.org/10.1016/j.ces.2015.07.015

Chemical Engineering Science 137 (2015) 1014–1023

Contents lists available at ScienceDirect

Chemical Engineering Science

journal homepage: www.elsevier.com/locate/ces

Laminar mixing in a SMX static mixer evaluated by positron emission particle tracking (PEPT) and magnetic resonance imaging (MRI)

Olga Mihailova [a], Victor Lim [b,1], Michael J. McCarthy [b], Kathryn L. McCarthy [b], Serafim Bakalis [a]

[a] School of Chemical Engineering, University of Birmingham, Birmingham B15 2TT, UK
[b] Department of Food Science and Technology, University of California, Davis, Davis, CA 95616, USA

HIGHLIGHTS

- Two experimental techniques are combined for quantitative measure of mixedness.
- Mixing is more effective in the initial elements of the SMX than predicted from CFD.
- Combination of MRI and PEPT techniques opens a range of complementary studies.

ARTICLE INFO

Article history:
Received 9 March 2015
Received in revised form
4 July 2015
Accepted 6 July 2015
Available online 30 July 2015

Keywords:
Mixing
Static mixer
Velocity
Newtonian
Positron emission particle tracking (PEPT)
Magnetic resonance imaging (MRI)

ABSTRACT

Static mixers are implemented across many industries and are used for mixing, heating and reacting processes. This paper reports the combined use of positron emission particle tracking (PEPT) and magnetic resonance imaging (MRI) to assess mixing in the industrially important SMX static mixer geometry. The focus of this study was distributive mixing for a Newtonian fluid, glycerol, flowing in the laminar regime in the standard SMX static mixer. By implementing PEPT and MRI techniques, the work elucidated mixing indices that incorporate both local velocities and concentration fields within the structure of the mixer element at 0.5 mm intervals over a length of nine 1.0L/D SMX elements. The experimental results are placed in context with previously published computational studies for this geometry.

1. Introduction

The shift towards continuous processing is ever increasing, as it allows for more streamline and cost effective manufacturing. Continuous processing reduces energy consumption and waste production when compared to an equivalent amount of product manufactured by batch methods. As many of these processes rely on mixing and heat transfer, static mixers are increasingly incorporated into processing systems (Etchells III and Meyer, 2004; Ghanem et al., 2014). The insert-type configuration of the static mixer redistributes fluid flow in directions transverse to the main flow due to a series of motionless inserts, or elements. This type of distributive mixing is by convection rather than diffusion. The focus of this study was distributive mixing for a Newtonian fluid flowing in the laminar regime for a specific type of static mixer, the standard SMX static mixer (Sulzer Chemtech, Winterthur, Switzerland).

The SMX mixer has been the subject of a number of experimental and computational studies, well summarized by Thakur et al. (2003), Singh et al. (2009), and Meijer et al. (2012). Significant strides have been made using computational fluid dynamics (CFD) and the mapping method to assess performance of the SMX mixer (Rauline et al., 2000; Zalc et al., 2002; Liu et al., 2006; Singh et al., 2009). In general (but not without exception), computational results have been challenging to validate or to compare with experimental mixing performance due to the geometrically complex nature of the mixing system. In a proof of concept portfolio paper, Leschka et al. (2007) illustrated simultaneous measurements using planar laser-induced fluorescence (PLIF) and particle image velocimetry (PIV) for flow behind the SMX static mixer.

This paper introduces two different experimental techniques that are combined to evaluate the qualitative and quantitative

E-mail addresses: OXM186@bham.ac.uk (O. Mihailova), victor.lim@agilent.com (V. Lim), mjmccarthy@ucdavis.edu (M.J. McCarthy), klmccarthy@ucdavis.edu (K.L. McCarthy), s.bakalis@bham.ac.uk (S. Bakalis).
[1] Present address: Agilent Technologies, Inc., Santa Clara, CA 95051, USA.

http://dx.doi.org/10.1016/j.ces.2015.07.015

measure of mixedness through the SMX mixer: positron emission particle tracking (PEPT) and magnetic resonance imaging (MRI). Positron emission tomography (PET) and MRI have been combined to utilize their complementary abilities to enhance medical diagnostics (Zaidi and Del Guerra, 2011; Herzog, 2012). Small scale PET/MRI systems have recently become available for use in preclinical research (Anonymous, 2014). PEPT, a technique developed in the University of Birmingham, allows non-invasive spatial tracking of a neutrally buoyant radioactive labelled tracer particle (Parker et al., 1993; Eesa and Barigou, 2008). This technique has been successfully used to characterize a number of industrial processes, such as tumbling mills (Volkwyn et al., 2011) and stiller vessels (Chiti et al., 2011), as well as a number of domestic appliances, washing machines (Mac Namara et al., 2012) and dish washers (Pérez-Mohedano et al., 2014). The technique relies on tracking a single neutrally buoyant particle through the system. As the particle emits back to back γ-rays, the location of the tracer can be accurately triangulated by the PEPT algorithm at short time intervals, in the order of microseconds, which consequently allows calculating the 3D velocity of the tracer. The technique depends on recirculating the tracer until the particle passes sufficiently cover the volume of the system (Parker et al., 1993).

Nuclear magnetic resonance (NMR) and magnetic resonance imaging (MRI) are spectroscopic techniques that are based on the interaction between nuclear magnetic moments and applied external magnetic fields. These techniques are used to measure composition, structure, molecular mobility, molecular diffusion and bulk material motion. Discussion of the techniques and applications are given in McCarthy and McCarthy (2013, 2014). MRI studies of mixing processes have been reported in the literature for both batch and continuous systems. Representative studies from the University of California, Davis lab include: McCarthy and McCarthy (2000), Lee et al. (2001), McCarthy et al. (2002) and Choi et al. (2004). Relevant to this SMX static mixer work, Tozzi et al. (2012, 2013) and Lim et al. (2015) reported the use of MRI to characterize mixing at low Reynolds number in static mixers. These studies are performed by introducing components with different magnetic relaxation properties. For flow studies that involve the mixing of multiple fluid streams, the use of a small amount of NMR contrast agent, such as manganese chloride or gadolinium chloride, is common since it does not significantly alter flow properties of the fluid. Changes in NMR signal intensity (SI) are attributed to the mixing of the fluid streams. With calibration techniques, the 2D MR images are converted to concentration maps. In addition, direct velocity imaging in a SMX-type static mixer has been reported by Herold et al. (2015), for the primary purpose of identifying dead zones in the mixing geometry.

By implementing PEPT and MRI techniques, the current work reports an assessment of both local velocities and concentration fields within the structure of the mixer element. Conventional statistical methods are presented to illustrate mixing as a function of axial position within the SMX mixer. Lastly, the experimental results from both techniques are combined in a flux-weighted intensity of segregation as a measure of homogeneity.

2. Materials and methods

2.1. Materials

2.1.1. Test fluid

Glycerol, a model Newtonian fluid, was utilized as the test fluid for MRI and the PEPT trials. In the case of PEPT experiments unmodified glycerol was used, with a single neutrally buoyant tracer particle. Pure glycerol was acquired from Reagent (Cheshire, UK); glycerol rheology was characterized using a rotational rheometer (AR 1000, TA Instruments, UK) yielding a viscosity of 1.262 ± 0.005 Pa s.

For MRI experiments, glycerol (Essential Wholesale and Lab, Portland, OR) was doped with the NMR contrast agent, gadolinium chloride ($GdCl_3$) (Sigma Aldrich, St. Louis, MO). Two levels of doping were used to provide SI contrast between two fluid streams: 4×10^{-4} M and 20×10^{-4} M $GdCl_3$ in glycerol. These levels of doping minimize change in physical properties of the test fluid while altering the NMR signal intensity values. For simplicity, the higher level of doping at 20×10^{-4} M $GdCl_3$ in glycerol is referred to as "doped". The rheology of these solutions were characterized using a rotational rheometer (Bohlin CVO, Malvern Instruments, UK) yielding viscosities of 0.950 ± 0.004 Pa s and 0.920 ± 0.008 Pa s.

Rheological differences between the glycerol used for PEPT and for MRI trials can be attributed to the different suppliers and the addition of the contrast agent.

2.1.2. SMX mixer

Static mixers are effective pipeline devices in the laminar flow regime. Etchells III and Meyer (2004) provide an excellent discussion of design and application of various types of inline mixing. The SMX mixer, initially developed jointly by Koch and Sulzer, is an ideal choice for mixing/blending of miscible fluids of similar or dissimilar viscosities. The DN25 SMX (1″) elements were used in both MRI and PEPT trials. The SMX element has a diameter of 25.4 mm and a length of 25.4 mm, for a length to diameter ratio (L/D) of 1.0. It is comprised of six planes of 3.18 mm × 1.9 mm bars spaced 3.18 mm apart. Three planes of bars are spaced 9 mm apart with the remaining three planes placed orthogonally. The axial direction is offset 45° from both sets of planes. Each consecutive element is oriented at 90° to the preceding one, alternating the direction of fluid flow through the mixer, achieving the desired stretch and fold mixing mechanic characteristic of the SMX mixers (Zalc et al., 2002). This geometry is typically described as the "standard" SMX (2, 3, 8) design with 2 units over the height of the channel, 3 parallel bars along the length of one element and 8 cross bars over the width of the channel (Fig. 1).

Although industrial mixing applications typically use metals as the material of construction, metal cannot be used in the MR magnet since it distorts or shields signal from the hydrogen nuclei in the fluid. Though the PEPT technique does not have the same constraint, the plastic elements cause less scattering, as the γ-rays pass more readily through plastic than metal (Mansfield and O'Sullivan, 2010). Therefore, the elements for both the MRI and PEPT studies were constructed from plastic.

For the MR study, individual plastic elements of ABS-like (thermoplastic acrylonitrile–butadiene–styrene) material were purchased from Sulzer Chemtech USA Inc. (Tulsa, OK). Nine SMX elements were secured in a Schedule 40 transparent plastic tube as described above. A flat flow splitter that spanned the diameter of the tube was inserted into the tube upstream of the first SMX element to isolate the two test fluids in two semi-elliptic channels.

For the PEPT trials, two 5-element SMX mixers were 3D-printed by TEAM Design, Prototyping, and Fabrication Laboratory (University of California, Davis) based on CAD drawings of the ABS-like SMX element. The material of construction was Objet VeroClear (a transparent acrylic compound; Stratasys, Eden Prairie, MN).

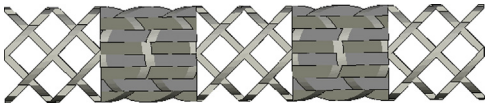

Fig. 1. CAD diagram of five consecutive elements of a standard SMX mixer.

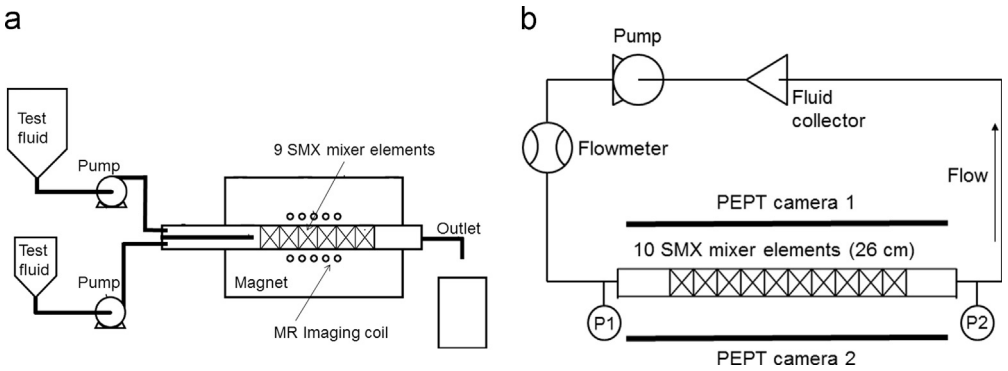

Fig. 2. Schematic representation of the experimental setup for (a) MRI trials, (b) PEPT trials.

2.2. Methods

2.2.1. MRI technique

Fig. 2a gives a schematic representation of the experimental setup for the MRI trials. The nine-element SMX mixer assembly was centred in the imaging section of a 1 T permanent magnet. MR imaging was performed using an Aspect Imaging spectrometer with a 0.3 T/m peak gradient strength (Shoham, Israel). The radio frequency coil was a solenoid with four turns, encasing a cylindrical volume of 60 mm in diameter and 60 mm in length.

Two positive displacement pumps (FH100X Peristaltic Pump, Thermo Scientific, Fisher Scientific, Houston, TX) pumped the test solutions from two reservoirs at a constant volumetric flow rate of 2.7 mL/s each to achieve a 50:50 ratio of the two fluids. The combined flow rate was 5.4 mL/s into the SMX mixer for a Reynolds number of 0.4 in the open pipe. Both glycerol-based test fluids were pumped through the mixer until steady flow was achieved. The pumps were then simultaneously stopped and MR images were obtained using a multi-slice gradient recall echo sequence in the sagittal orientation on the stationary fluid. The MR parameters were repetition time (TR) of 5.7 ms, echo time (TE) of 1.9 ms, slice thickness of 0.5 mm, and 128 slices, yielding an image resolution of 0.313 mm. Once a set of images was acquired normal to the flow direction at a given axial location, the SMX mixer was moved to image a downstream axial position. The pumping and imaging procedure was repeated at the new axial position. The flow system was single pass and the fluids were not recirculated. Calibration vials with 6 different levels of dopant were prepared and MR imaged to a obtain calibration curve that quantified the SI at different mixtures of the two test fluids (4 replicates). The relationship between the signal intensity and level of gadolinium chloride was linear with a coefficient of determination of 0.94.

2.2.2. MRI data processing

The MR images were standardized to provide a means of image to image comparison. Experimental noise was addressed first. For each image signal from void regions (regions of air or plastic) were zeroed so their values did not contribute to the sum of signal intensities of the image. Signal intensities arising from fluid in contact with the plastic of the SMX element or tube wall were also zeroed to eliminate the effect of partial volume averaging. The remaining SI values were nonzero values solely due to signal from fluid.

Signal intensities were then converted to percentage of doped test fluid with the linear regression equation of the calibration curve, yielding values from 0 to 100. Each image was then divided by its average value to yield images that had exactly an average of 50% doped fluid. All images in each set were then divided by the maximum SI of the set and multiplied by 100 to yield a range of values between 0 and 100. The last procedure was performed to acknowledge that unmixed fluid had a distribution of signal intensities. Dividing by the maximum signal intensity was dividing by the value that was essentially three standard deviations above the mean of the high SI test fluid. The images were cropped to 83×83 pixels to accommodate comparison to PEPT data. MATLAB 2013a (The MathWorks, Inc., Natick, MA) was used to perform image and data analysis.

2.2.3. PEPT technique

As PEPT technique relies on tracking a single neutrally buoyant tracer particle at any given time, a closed loop system was used, which allowed recirculation of the fluid seeded with the tracer (Eesa and Barigou, 2008). A schematic representation of the experimental setup for the PEPT trials is shown in Fig. 2b. A plastic pipe 1 in. ID (26 mm) was used with 10 plastic SMX mixer elements located in the middle of the pipe. The mixer section of the system was positioned centrally in the field of view of the PEPT apparatus, allowing open pipe regions to be present in the field of view. For all experiments, the flow rate was controlled at 300 L/h for a Reynolds number of 5.5 in the open pipe. Pressure and temperature in the pipeline were monitored and logged using a pair of pressure/temperature transducers located either side of the PEPT field of view.

Fluid was circulated using a flexible impeller pump, minimizing the stress exerted on the tracer particle, prolonging its stability and reducing contamination of the bulk fluid with radioactive material. By minimizing the total volume of the system to 3 L it was possible to achieve a particle pass through the field of view approximately every 90 s. The experiment had to be reset every 3 h due to degradation of particle activity and bulk contamination, until a minimum of 800 particle passes were recorded achieving sufficient coverage at all radial positions across both the open pipe and the static mixer regions.

2.2.4. PEPT data processing

Processing the raw data collected by the PEPT cameras yields sets of x–y–z coordinates with respect to time. These data points were rotated in a way that aligns the internal structure of the mixer with the Cartesian coordinate planes. The resulting sets of coordinates were separated into individual particle passes, based on the time delay between consecutive detections, as the time between detections in the same pass is on the order of milliseconds, while the time it takes for the particle to recirculate into the field of view after a pass was over a minute. A number of typical particle passes with respect to time and spatial direction are illustrated in Fig. 3, where it can be seen that the particle travels extensively across both the x and the y planes, perpendicular to the flow, but follows a steady pattern in the direction

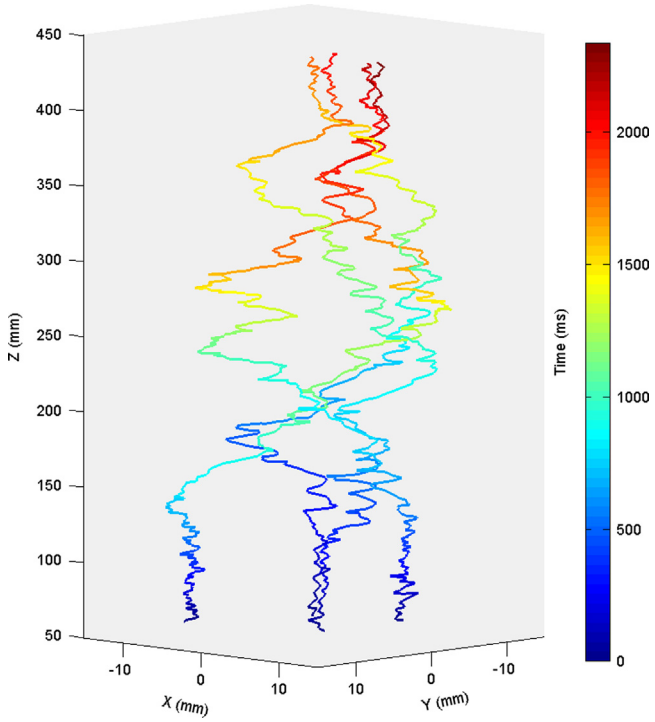

Fig. 3. Four typical particle passes, where the position of the particle along the *x*-, *y*-, and *z*-axes is illustrated against time from the moment the particle enters the field of view.

Table 1
Average particle pass statistics, showing number of detections used for location triangulation, residence time, locations detected per particle pass, time between detections and divergence from laminar flow in the empty pipe region.

Parameter	Value
Number of γ-ray pairs used for location triangulation (–)	125 ± 12
Residence time (s)	2.52 ± 0.66
Locations per particle pass (–)	315 ± 70
Time between detections (ms)	8 ± 2
Divergence from flow in the laminar region of the pipe (mm)	0.55 ± 0.20

parallel to the flow. No back mixing was observed in the system and the velocity component in the *z* direction was always positive. Table 1 summarizes a typical particle pass, where it can be seen that on average detection occurred every 8 ms, resulting in approximately 315 particle locations per pass.

Particle spatial location data with respect to time allowed estimates of local velocities. PEPT was previously shown to characterize velocity distributions within simple and complex geometries (Mac Namara et al., 2012; Bakalis et al., 2004). By the same approach, the *x*-, *y*-, *z*-velocity components were estimated for the current system. A second order polynomial was fit to a set of 7 points along each of the axis as a function of time, describing the path of the particle in time:

$$i = at^2 + bt + c \tag{1}$$

where *i* represents the *x*, *y* or *z* direction component, *t* is time and *a*, *b* and *c* are constants. The resulting polynomial was differentiated, yielding the rate of change of displacement with respect to time in a given direction, i.e. velocity component:

$$U_i = \frac{di}{dt} = 2at + b \tag{2}$$

where the constants are as in Eq. (1). The individual velocity components were then combined to give the overall velocity of the fluid, *U*:

$$U = \sqrt{U_x^2 + U_y^2 + U_z^2} \tag{3}$$

The velocity profile of Newtonian fluid flowing under laminar conditions in a simple geometry can be estimated theoretically (Chhabra and Richardson, 2008). Agreement between theoretical profiles and the local velocities obtained through PEPT data analysis indicates that when more complex geometries or fluids are considered, the velocities tracked using PEPT are valid (Bakalis et al., 2004; Marigo et al., 2013).

In order to assess mixing, individual passes were labelled differently depending on the location of the particle as it was entering the first SMX element, with traces entering on one side of the pipe midpoint assigned the equivalent of the high contrast intensity, and the low contrast intensity assigned to the tracers entering on the other side. This procedure allowed effective separation of the flow into two streams, with a 50:50 volumetric ratio of the two fluids, in a manner similar to the MRI trials described previously (cf. Section 2.2.1). Furthermore, to increase the detection density across one element the 10 element mixer was "cut up" into individual elements based on the dimensions of system. These 10 individual elements were then rotated accordingly and superimposed, condensing all experimental data into one element. This resulted in the number of passes through the element to rise to over 6000, allowing for a more detailed characterization of both the mixing patterns and velocity fields within the element.

In addition, PEPT data were viewed as slices in the same fashion as MRI data allowing for side by side comparison. The SMX element resulting from superimposing all experimental data was divided into 0.5 mm slices and within each slice an 83×83 element grid with a $0.313 \times 0.313\ \text{mm}^2$ resolution was applied. Each grid segment contained the information for the given area of the cross-section, including spatial location, time of detection and the concentration value for each particle pass based on its entry location to the collated element. MATLAB 2013a (The MathWorks, Inc., Natick, MA) was used to perform image and data analysis.

3. Results and discussion

3.1. MRI results

Fig. 4 illustrates representative MR images for the first SMX element. The images are arranged from left to right, top to bottom at the designated axial positions. The colour map for each image is the same with high signal intensity fluid (red) flowing from the upper semi-elliptic channel into the SMX mixer and the low signal intensity fluid (aqua) flowing from the lower semi-elliptic channel into the SMX mixer at $z=0$. The dark blue regions within the cross section are due to the SMX geometry where plastic does not contribute to NMR signal and the signal intensity has been zeroed. Background regions, as well, are zero signal intensity values and given as dark blue. Each image is an additional 1/8 of a *L*/*D* downstream. As fluid moves downstream the mixer blades distort the initial region of doped fluid into spade-like structures that extend the cross-section of the mixer. Striations in the fluids become more pronounced as the fluid progresses through the element. Qualitatively these images are strikingly similar to the computed mixing patterns given in Zalc et al. (2002; Fig. 9) in their study of laminar flow and mixing of a Newtonian fluid in a SMX mixer assessed by computational techniques.

First and second order statistics quantify the extent of mixing. In particular, the intensity of segregation and coefficient of variation incorporate the variance s^2 and its square root, the standard

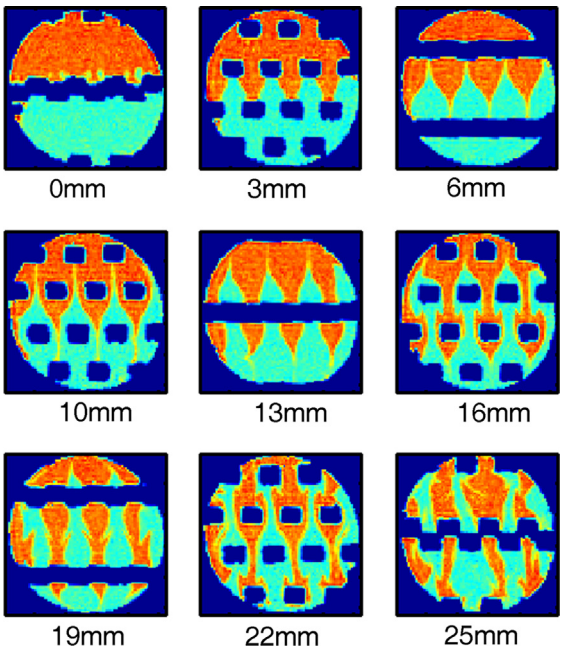

Fig. 4. MR images of the 2 glycerol streams at 50:50 volume ratio in the first SMX element.

deviation (s) as spread characteristics. The intensity of segregation, I, is defined as

$$I = \frac{s^2}{s_0^2} \tag{4}$$

where s_0^2 is the initial variance. The coefficient of variation (CV) is defined as

$$CV = \frac{s}{\overline{X}} \tag{5}$$

where the mean concentration, $\overline{X}$, is the mean signal intensity of the standardized MR image. Due to the standardization procedure (describe in Section 2.2.2), the mean for each image was the same value at 59.4.

Fig. 5a illustrates MR images of the mixing of the two glycerol streams at a position 3 mm into each of the 9 consecutive SMX elements. For the two glycerol solutions, the striations in the fluid are visually distinct through the fourth SMX element (at a distance of 79 mm). By the fifth element the two fluids have mixed to visual resolution. Fig. 5b gives histograms for each position in Fig. 5a. Initially the SI peaks are centred at values of 42 and 77. The bimodal distribution becomes unimodal centred at 61 and the standard deviation subsequently decreases from 10 to 4.

Quantitatively, the entire set of 520 MR images are described by intensity of segregation, coefficient of variations and length scale as a function of position given as L/D (Fig. 6). The values of these statistics were calculated for images upstream of the SMX mixer in the 2 semi-elliptic flow channels and are plotted as values at negative L/D prior to the SMX mixer. Intensity of segregation values in Fig. 6a drop linearly over the first three SMX elements and level off at approximately 0.08, whereas the intensity in the open pipe downstream of the static mixer was 0.04. In other words, the last few points in Fig. 6a illustrate the resolution of the image. Fig. 6b illustrates the coefficient of variation on a semi-logarithmic plot. The calculated maximum CV for the MR images at $L/D=0$ was 0.30, [Eq. (5)]. As fluid travelled through the SMX elements, the CV dropped from 0.30 to approximately 0.10. Further downstream, the CV of fluid in the open pipe was 0.06, again yielding an indication of the resolution of the image. For context,

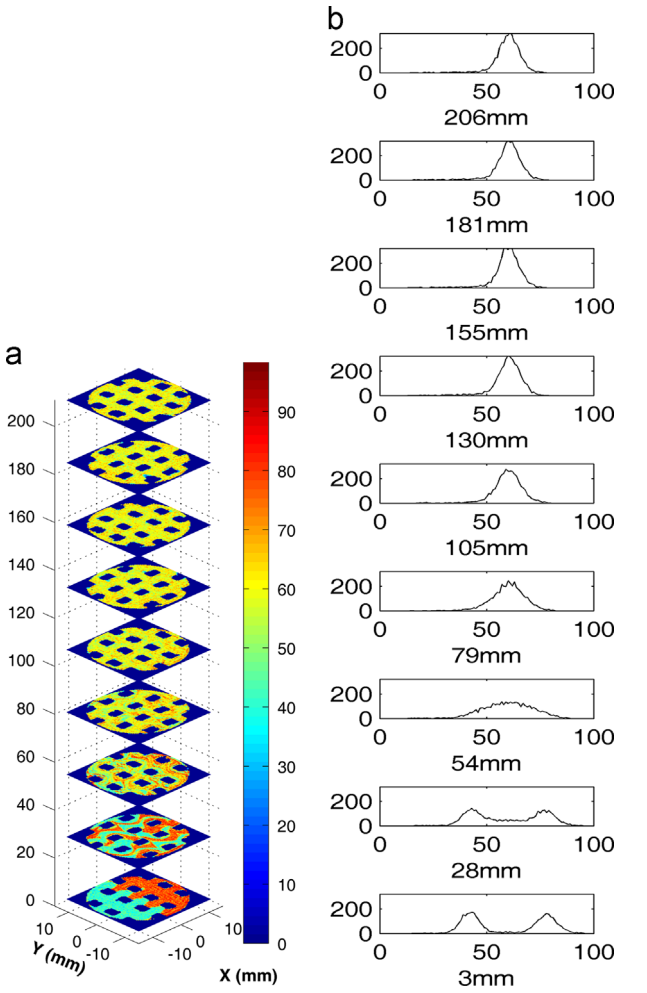

Fig. 5. Mixing of the 2 glycerol streams at 3 mm into consecutive SMX elements (a) MR image and (b) corresponding histograms.

Fig. 6b incorporates data taken from Etchells III and Meyer (2004; Fig. 7-5) to illustrate homogeneity in the SMX mixer when an additive is introduced at the middle of the pipe at a level of 50%. It is important to note that the coefficient of variation for an unmixed sample given by statistical theory and based on unmixed volume fraction is 1.0 at $L/D=0$. In contrast, experimentally coefficient of variation is considerably lower as initial SI data take values other than completely unmixed (for instance, at solely 0 or 1).

The scale of segregation, or the length scale, is a second order statistic and was calculated for each image. This statistic is based on the coefficient of correlation:

$$R(r) = \frac{\sum_{i=1}^{N}(X_A - \overline{X})(X_B - \overline{X})}{Ns^2} \tag{6}$$

where X_A and X_B are concentrations separated by r, $\overline{X}$ is the mean concentration, and N is the number of X_A and X_B pairs separated by distance r. Values of R are calculated for all values of r. These values are integrated for the length scale:

$$S_L = \int_0^{\xi} R(r)dr \tag{7}$$

where ξ is at $R(r=\xi)=0$ (Tadmor and Gogos, 2006). Length scale values as a function of L/D are plotted in Fig. 6c. The lower the length scale, the better the two fluids have mixed in the cross section. Similar to the intensity of segregation, rapid and dramatic

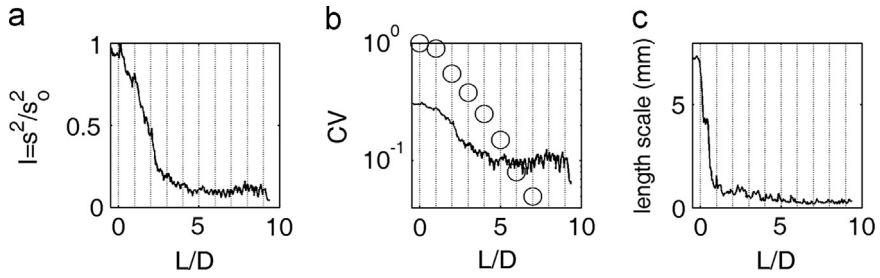

Fig. 6. Mixing statistics based on MR images as a function of L/D for (a) intensity of segregation, (b) coefficient of variation with data (○) from Etchells III and Meyer (2004), and (c) length scale.

change occurs over the first three SMX elements and then a more gradual decrease in length scale values.

The intent of this research was to assess both local velocities and concentration fields within the structure of the SMX mixer element. PEPT results are now introduced and then the two experimental techniques combined.

3.2. PEPT results

PEPT data can be used to estimate a number of properties of a system, such as velocities, concentrations, flow patterns and local shear fields (Bakalis et al., 2004; Mac Namara et al., 2012). For the purposes of this research the focus was on concentration and velocity fields. As mentioned previously, due to the nature of the technique and the tracer particle, the mixer inlet was labelled as necessary by identifying individual particle passes. In order to match the experimental setup used for MRI, the feed was divided into two equal streams based in the axial position of the tracer particle at the inlet of the first mixer element. Consequently, depending on the position of the tracer the particle pass was assigned an initial concentration value of either 40 or 80 in the first cross section, depending on the location. In the consequent slices (that is, cross sections), the concentration was calculated by dividing the x–y plane into 83×83 element grid and taking the average concentration of all the passes present in each segment of the grid. The concentration changes and the degree of mixing were then assessed in a manner similar to that applied for the MRI data processing. Fig. 7 illustrates the MRI concentration images (Fig. 7a) and PEPT concentration images (Fig. 7b) through the first SMX element; qualitative agreement with the MRI results, as well as with the CFD results of Zalc et al. (2002) provided confidence in the PEPT tracking algorithm and the approach to trace individual particle passes.

The power of PEPT was to acquire local velocities of the fluid as it travels through the SMX mixer. Local velocity fields offer an improved understanding of the mixing mechanisms and can further be used to determine other properties of the system, such as local shear rate distribution, which play an important role when processing shear sensitive fluids.

The velocity field within the SMX mixer was dictated by the geometry of the mixer. Due to the orientation of the blades, laminar mixing occurs only along the axes perpendicular to the flow. This flow pattern for the velocity along the x-axis is shown in Fig. 8a. Velocity values ranged between -0.3 and 0.3 m/s, with the maximum velocity at the centre of each gap. The symmetric probability functions that arise in this plane are consistent with those reported in the radial and azimuthal direction by Zalc et al. (2002).

It can be seen that even in regions of the mixer with no physical barrier, e.g. slices at 6 mm ($L/D=0.25$) and 12 mm ($L/D=0.5$), clear bands of fluid with opposite direction are present (Fig. 8a). This suggests that the fluid experiences significant shear forces as the streams with opposing direction flow past one another. In contrast, the direction of axial flow was always positive, with the maximum of 0.4 m/s reached in the middle of each gap between the mixer blades and the minimum of 0.05 m/s reached at the walls (Fig. 8b). Even though the velocity was expected to reach zero at the tube wall to satisfy the no slip condition, the particle was not observed to enter this boundary layer region, presumably due to its size.

Axial PEPT velocities maps at 4 planes were selected: 0.25L/D, 0.50L/D, 0.75L/D, and 1.0L/D. Fig. 9 illustrates these maps as dimensionless velocities; the axial velocities from Fig. 8 are dimensionless with the average velocity at the specified axial location, at the volumetric flow rate of 300 L/h. With the exception of 1.0L/D, the average velocity in the planes was roughly 0.2 m/s, about 20% greater than the average velocity in the open pipe at 0.16 m/s due to the geometry of the mixer. At 1.0L/D, the average velocity was 0.4 m/s since the effective cross sectional area was reduced further as fluid left one element and entered the next element. Histograms were constructed to view the velocity data in these planes in a quantitative way (Fig. 10a). The histograms are essentially centred at the dimensionless velocity of 1.0 and normally distributed. For comparison, the analytical velocity maps were calculated for the semi-elliptic channel and the open pipe. The semi-elliptic channel geometry was relevant for the flow upstream of the SMX mixer for the MRI trials. The 150 mm entrance length was sufficient to ensure fully developed flow for the glycerol streams. The analytical solution for this geometry was presented by Alassar and Abushoshah (2012) to describe flow through the semi-elliptic channel formed by the flat flow splitter. Hagen–Poiseuille flow in an open pipe was relevant for the flow downstream of the SMX mixer. Qualitatively the histograms for these geometries differ than those for the SMX mixer (Fig. 10b). The histogram for flow in the semi-elliptic channel is relatively flat over the dimensionless velocities from 0 to 2 as compared to the open pipe histogram that peaks at a dimensionless velocity of 2.0

Similar in concept to the histogram, probability distributions functions were given by Zalc et al. (2002; Fig. 8) for glycerol fluid properties in the SMX mixer at Reynolds numbers less than or equal to 10. In contrast to Fig. 10a, those distributions drop sharply at a dimensionless velocity of 1.7. The computational study also yielded a much larger fraction of dimensionless velocities in the range from 0 to 0.5. As stated above, though fluid velocity was expected to be zero at solid surfaces to satisfy the no slip condition, the PEPT particle was not observed to enter this boundary layer region, presumably due to its size. Therefore in the experimental study with PEPT, the lower velocities in a histogram should be expected to be somewhat underrepresented due to the technique.

3.3. PEPT and MRI results

Galaktionov et al. (2002) introduced flux-weighted intensity of segregation to assess mixing in a Kenics mixer. This group later applied the concept to SMX mixers with a recent article being

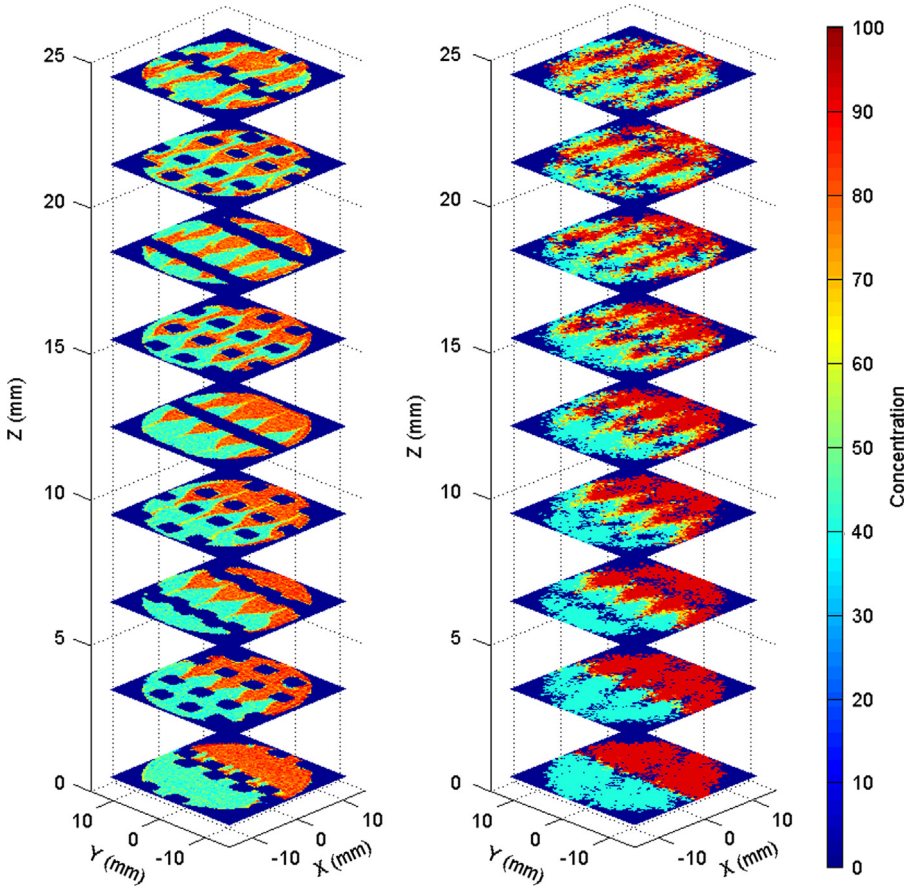

Fig. 7. Mixing patterns for the 2 glycerol streams at 50:50 volume ratio illustrated by (a) MR images and (b) PEPT particle pass tracking.

Meijer et al. (2012). The flux-weighted intensity of segregation incorporated both flow and concentration at cross sections of the mixer obtained through computational methods. As with the intensity of segregation given in Eq. (4), the flux-weighted intensity of segregation is the ratio of local variance to initial variance. The variance is now flux-weighted variance and is given by

$$s_F^2 = \frac{1}{F}\sum_{i=1}^{N}(X_i - \overline{X})^2 f_i \tag{8}$$

where f_i is the volumetric flux (that is, axial velocity) through pixel i and F is the total flux through the mixer. Eq. (8) is incorporated into the flux-weighted intensity of segregation:

$$I_F = \frac{s_F^2}{s_{Fo}^2} \tag{9}$$

For the same reason that the experimental coefficient of variation was used in this study (Fig. 6b), the initial variance in the denominator of Eq. (9) was also calculated from experimental concentration (that is, standardized signal intensity) data rather than statistical theory.

Due to the data analysis procedures for MRI and PEPT, images at the same axial location were 83×83 pixels and superimposable. Individual PEPT pixel velocities in an image corresponded to f_i in Eq. (8). Standardized MR signal intensity values corresponded to X_i in Eq. (8). For each of the 9 SMX elements in the MR study, pixel-by-pixel operations were performed using the corresponding PEPT image (Fig. 9) at $0.25L/D$, $0.5L/D$, $0.75L/D$ and $1.0L/D$ to yield the flux-weighted intensity of segregation at that position. Both the non-flux-weighted (Fig. 6a) and flux-weighted intensity of segregation are given in Fig. 11 on the more conventional semi-logarithmic axes. For this MR study with the two viscosity matched glycerol test solutions delivered to the SMX mixer at a 50:50 ratio, the non-flux-weighted and the flux-weighted intensity of segregation values are quite similar, with the exception that the flux-weighted values are subject to less fluctuation at L/D values greater than 4. Over the second, third and fourth elements, the values of the two statistics show a characteristic linear decrease on the semi-logarithmic scale.

As stated in Section 3.3, Meijer et al. (2012) incorporated flux-weighted intensity of segregation as part of the quantitative comparison of different types of static mixers. The intent of that study was to provide assessment on the performance of industrially relevant static mixers; the comparison of performance within the study is more relevant than comparison to this work. Nonetheless, values of flux-weighted intensity of segregation for a standard SMX (2, 3, 8) taken from their Fig. 11 (Meijer et al., 2012) are plotted in Fig. 11. The experiment results from MRI and PEPT indicate more rapid mixing along the axial length than resulted with the mapping method. However, the experimental data plateau at the resolution of the image, which was not a constraint in the computational technique.

3.4. PEPT and MRI comparison

These two experimental techniques have been utilized to characterize mixing and the data are in excellent agreement for equivalent experimental setups. The strength of the PEPT technique is the ability to measure particle velocities which are used to calculate both velocity and concentration as a function of position in the mixer. Metal structures may also be used in the PEPT apparatus. In contrast the strength of MRI is the ability to measure fluid concentration as a function of position. Only extremely limited uses of metal in the object to be imaged are possible

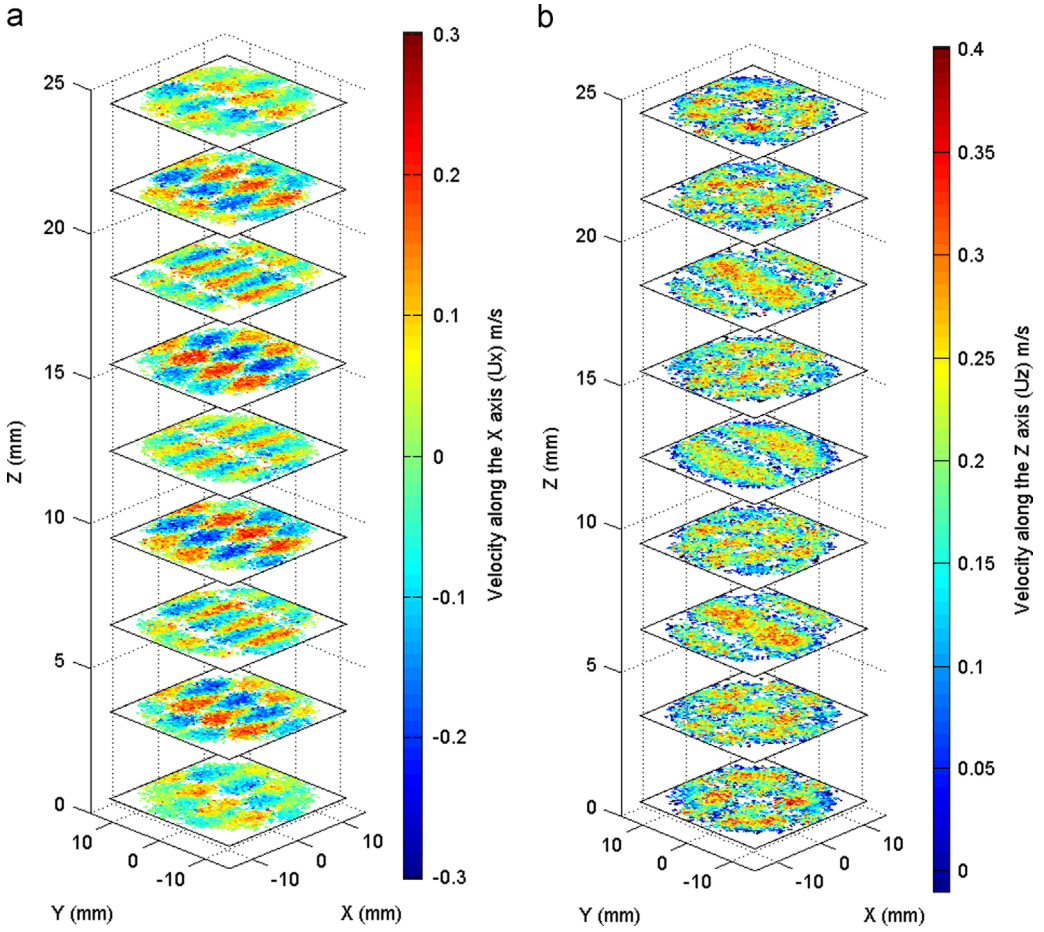

Fig. 8. Velocity distribution calculated from PEPT data (a) along the *x*-axis (U_x), perpendicular to the flow and (b) along the *z*-axis (U_z), parallel to the flow, at 3 mm increments within an SMX element for glycerol at 300*L*/*D*

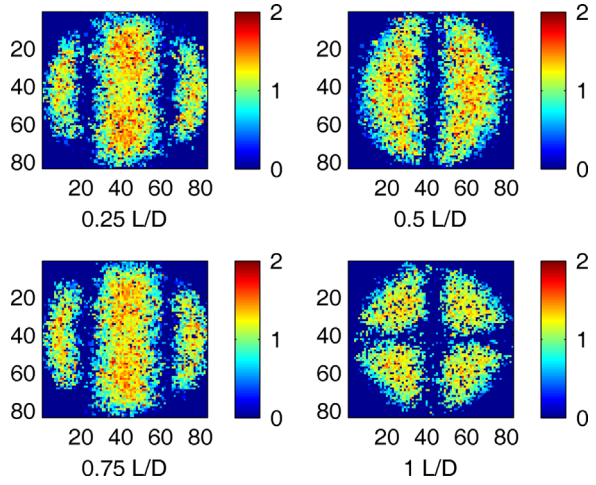

Fig. 9. PEPT axial velocity images at 0.25*L*/*D*, 0.5*L*/*D*, 0.75*L*/*D* and 1.0*L*/*D*, dimensionless with the average velocity.

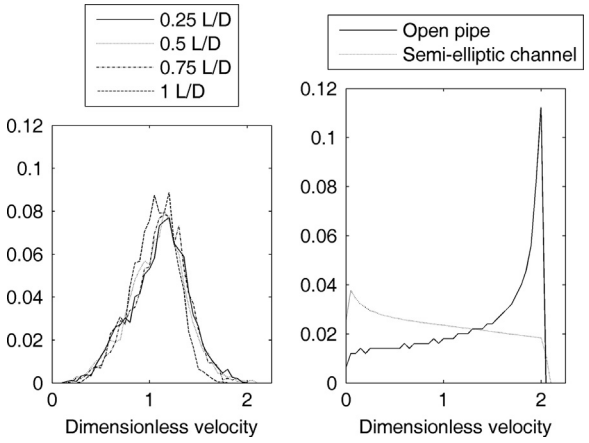

Fig. 10. Histograms for (a) PEPT data at the positions given in Fig. 9, and (b) analytical velocity maps for upstream and downstream geometries flows.

inside the MRI system and hence non-metallic structures are required for the mixing and piping network. To achieve the most accurate concentration measurements the fluid flow inside the MRI should be stopped during acquisition. Methods exist to flow compensate the data acquisition however the concentration results will likely have some degradation in accuracy (Callaghan, 2011). MRI may also be used to measure fluid velocity and molecular diffusion (Callaghan, 2011). In mixing of suspensions the potential exists to measure particle behaviour using PEPT and fluid behaviour using MRI permitting an almost complete characterization of the material and mixing process.

4. Conclusions

PEPT and MRI are powerful experimental techniques that can be employed, either separately or together, to study a variety of flow systems. By proper experimental design, the limitation of each technique was addressed. For MR, material of construction was

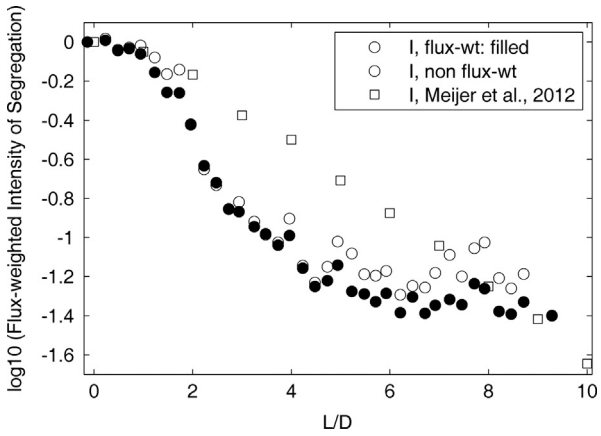

Fig. 11. Intensity of segregation as a function of L/D, (a) MR concentration data from Fig. 5a, (b) combining PEPT velocity data and MR concentration data, and (b) published flux-weighted intensity of segregation for the same geometry, Standard SMX (2, 3, 8).

non metal; for PEPT, the recirculation loop was designed to maximize the activity of the γ-ray emitting particle. MRI signal intensity data were successfully related to local component concentrations within the SMX static mixer. The resulting concentration images were discussed in terms of conventional mixing statistics. PEPT captured the real-time spatial location of the tracer particle which was interpreted in terms of both local concentration and velocity vectors. The PEPT technique offers the advantage of future analysis of velocity gradients and shear rate distribution within the mixer. The discussion of laminar mixing in the SMX was enhanced by the incorporation of PEPT velocity information and MR concentration information in the flux-weighted intensity of segregation. Comparisons of the results of this study were made to computational studies performed with CFD and the mapping method. CFD concentration maps and MR images are qualitatively and quantitatively similar with respect to the development of "spade-like" structures and the spatially-periodic chaotic flow. The mapping method provided an excellent means to combine local velocity and concentration information in a single statistic, the flux-weighted intensity of segregation. The experimental data from PEPT and MRI suggest that mixing is more effective in the initial stages of the SMX mixing elements than predicted from CFD and that shorter length static mixing sections could achieve desired results.

The ability to combine these two techniques, MRI and PEPT, opens a range of possibilities for future complementary studies. For example the techniques can be combined to evaluate slurries in complex processing geometries, where MRI is used to track the liquid component of the slurry while the PEPT tracer particle represents the suspended solids, resulting in a full characterization of the system. Additional MRI based measurement could be added to characterize colloidal structures and material domain sizes further extending the description of the state of a system. With the recent introduction of a commercially available combined PET/MRI spectrometer and the continued research efforts to integrate the two technologies the cost associated with the equipment should be significantly reduced in the future. Lower cost of this type of combined spectrometer will enable the transition into more applications in process analysis and process control.

Acknowledgement

We gratefully acknowledge the support of the Engineering, Physics and Science Research Council (EPSRC, Grant No. EP/L015153/1) and the help of Dr. Thomas Leadbeater and Prof. David Parker from the School of Physics and Astronomy at the University of Birmingham for preparing radioactive tracers and using the PEPT equipment. In addition, we acknowledge Procter & Gamble BIC for partially funding the project and supporting this publication, in particular Dr. Denis O'Sullivan, Christopher Jones, Walter Broeckx and Pascal Dossin for their personal interest in this work. We appreciate the support of Aspect Imaging, LLC for supplying pulse sequences and radio frequency coils for this work.

M. McCarthy is a consultant to Aspect Imaging, LLC.

References

Alassar, R.S., Abushoshah, M., 2012. Hagen–Poiseuille flow in semi-elliptic microchannels. J. Fluids Eng. – Trans. ASME 134 (12), 124502 (4 pp.).

Anonymous, 2014. Aspect Imaging's M2™ High-performance Compact MRI System including Novel Magnet and Gradients are Used to Power Mediso's NanoScan™ Integrated Whole-body Pre-clinical PET-MR and SPECT-MR Systems for In-line Multimodality Pre-clinical Imaging. ⟨http://www.aspectimaging.com/pre-clinical/product/mediso-nanoscan⟩, July 4, 2015.

Bakalis, S., Fryer, P.J., Parker, D.J., 2004. Measuring velocity distributions of viscous fluids using positron emission particle tracking (PEPT). AIChE J. 50 (7), 1606–1613.

Callaghan, P.T., 2011. Translational Dynamics & Magnetic Resonance Principles of Pulsed Gradient Spin Echo NMR. Oxford University Press, New York.

Chhabra, R.P., Richardson, J.F., 2008. Non-Newtonian Flow and Applied Rheology: Engineering Applications, 2nd ed. Butterworth-Heeinemann/Elsevier, Amsterdam.

Chiti, F., Bakalis, S., Bujalski, W., Barigou, M., Eaglesham, A., Nienow, A.W., 2011. Using positron emission particle tracking (PEPT) to study the turbulent flow in a baffled vessel agitated by a Rushton turbine: improving data treatment and validation. Chem. Eng. Res. Des. 89 (10), 1947–1960.

Choi, Y.J., McCarthy, M.J., McCarthy, K.L., 2004. MRI for process analysis: co-rotating twin screw extruder. J. Process Anal. Chem. 9 (2), 72–85.

Eesa, M., Barigou, M., 2008. Horizontal laminar flow of coarse nearly-neutrally buoyant particles in non-Newtonian conveying fluids: CFD and PEPT experiments compared. Int. J. Multiph. Flow 34 (11), 997–1007.

Etchells III, A.W., Meyer, C.F., 2004. Mixing in pipelines. In: Paul, E.L., Atiemo-Obeng, V.A., Kresta, S.M. (Eds.), Wiley-Interscience, Hoboken, NJ, USA.

Galaktionov, O.S., Anderson, P.D., Peters, G.W.M., Meijer, H.E.H., 2002. Morphology development in a Kenics static mixers (application of the extended mapping method). Can. J. Chem. Eng. 80, 604–613.

Ghanem, A., Thierry, L., Della Valle, D., Peerhossaini, H., 2014. Static mixers: mechanisms, applications, and characterization methods – a review. Chem. Eng. Res. Des. 92 (2), 205–228.

Herold, H., Hardy, E.H., Brodhagen, A., Muller, C., Nestle, N., 2015. Direct velocity imaging by magnetic resonance in a static mixer model produced using stereo lithography. Chem. Eng. Sci. 134, 599–604.

Herzog, H., 2012. PET/MRI: challenges, solutions and perspectives. Z. Med. Phys. 22, 281–298.

Lee, Y., McCarthy, M.J., McCarthy, K.L., 2001. Extent of mixing in a two-component batch system measured using MRI. J. Food Eng. 50 (3), 167–174.

Leschka, S., Thevenin, D., Zahringer, K., Lehwald, A., 2007. Fluid dynamics and mixing behavior of a SMX-type static mixer. J. Vis. 10 (4), 342.

Lim, V., Hobby, A.M., McCarthy, M.J., McCarthy, K.L., 2015. Laminar mixing of miscible fluids in a SMX mixer evaluated by magnetic resonance imaging (MRI). Chem. Eng. Sci. , http://dx.doi.org/10.1016/j.ces.2015.07.003.

Liu, S., Hrymak, A.N., Wood, P.E., 2006. Design modifications to SMX static mixer for improving mixing. AIChE J. 52 (1), 150–157.

Mac Namara, C., Gabriele, A., Amador, C., Bakalis, S., 2012. Dynamics of textile motion in a front-loading domestic washing machine. Chem. Eng. Sci. 75, 14–27.

Mansfield, M., O'Sullivan, C., 2010. Understanding Physics, 2nd Ed. Wiley, Chichester.

Marigo, M., Davies, M., Leadbeater, T., Cairns, D.L., Ingram, A., Stitt, E.H., 2013. Application of positron emission particle tracking (PEPT) to validate a discrete element method (DEM) model of granular flow and mixing in the Turbula mixer. Int. J. Pharm. 446, 46–58.

McCarthy, K.L., Lee, Y., McCarthy, M.J., 2002. Magnetic resonance imaging as a sensor system for multiphase mixing. Applied Magnetic Resonance 22, 213–222.

McCarthy, K.L., McCarthy, M.J., 2000. MRI for process analysis: Kenics static mixer. J. Process. Anal. Chem. 5 (3,4), 94–103.

McCarthy, M.J., McCarthy, K.L., 2013. Ch. 25 Advanced sensors, quality attributes and modeling in food process control. In: Yanniotis, S., Taoukis, P., Stoforos, N. G., Karathanos, V.T. (Eds.), Food Engineering Series, Springer, New York.

McCarthy, M.J., McCarthy, K.L., 2014. Magnetic resonance imaging and nuclear magnetic resonance spectroscopy. In: O'Donnell, C., Fagan, C.C., Cullen, P.J. (Eds.), Springer, New York.

Meijer, H.E.H., Singh, M.K., Anderson, P.D., 2012. On the performance of static mixers: a quantitative comparison. Prog. Polym. Sci. 37 (10), 1333–1349.

Parker, D.J., Broadbent, C.J., Fowles, P., Hawkesworth, M.R., McNeil, P., 1993. Positron emission particle tracking – a technique for studying flow within engineering

equipment. Nucl. Instrum. Methods Phys. Res. Sect. A: Accelerators, Spectrometers, Detectors Assoc. Equip. 326 (3), 592–607.
Pérez-Mohedano, R., Letzelter, N., Amador, C., VanderRoest, C.T., Bakalis, S., 2014. Positron Emission Particle Tracking (PEPT) for the analysis of water motion in a domestic dishwasher. Chem. Eng. J. 259, 724–736.
Rauline, D., Le Blevec, J.-M., Bousquet, J., Tanguy, P.A., 2000. A comparative assessment of the performance of the Kenics and SMX static mixers. Trans. IChemE 78 (Part A), 389–396.
Singh, M.K., Anderson, P.D., Meijer, H.E.H., 2009. Understanding and optimizing the SMX static mixer. Macromol. Rapid Commun. 30 (4–5), 362–376.
Tadmor, Z., Gogos, C.G., 2006. Principles of Polymer Processing, 2nd Ed. John Wiley & Sons, Inc., Hoboken, NJ, USA.
Thakur, R.K., Vial, Ch., Nigam, K.D.P., Nauman, E.B., Djelveh, G., 2003. Static mixers in the process industries – a review. Trans. IChemE 81 (Part A), 787–826.
Tozzi, E.J., Bacca, L.A., Hartt, W.H., McCarthy, M.J., McCarthy, K.L., 2013. Study of multi-lamination of a non-Newtonian fluid in a spit and recombine mixer using magnetic resonance imaging. Chem. Eng. Sci. 93, 140–149.
Tozzi, E.J., McCarthy, K.L., Bacca, L.A., Hartt, W.H., McCarthy, M.J., 2012. Quantifying mixing using magnetic resonance imaging. J. Vis. Exp. 59, e3493. http://dx.doi.org/10.3791/3493.
Volkwyn, T.S., Buffler, A., Govender, I., Franzidis, J.-P., Morrison, A.J., Odo, A., van der Meulen, N.P., Vermeulen, C., 2011. Studies of the effect of tracer activity on time-averaged positron emission particle tracking measurements on tumbling mills at PEPT Cape Town. Miner. Eng. 24 (3-4), 261–266.
Zaidi, H., Del Guerra, A., 2011. An outlook on future design of hybrid PET/MRI systems. Med. Phys. 38 (10), 5667–5689.
Zalc, J.M., Szalai, E.S., Muzzio, F.J., Jaffer, S., 2002. Characterization of flow and mixing in an SMX static mixer. AIChE J. 48 (3), 427–436.